Phys. Status Solidi A **214,** No. 4, 1600425 (2017) / **DOI** 10.1002/pssa.201600425

physica status solidi a
www.pss-a.com
applications and materials science

Optimum structures for gamma-ray radiation resistant SiC-MOSFETs

Satoshi Mitomo*[,1,2], Takuma Matsuda[1,2], Koichi Murata[1,2], Takashi Yokoseki[1,2], Takahiro Makino[2], Akinori Takeyama[2], Shinobu Onoda[2], Takeshi Ohshima[2], Shuichi Okubo[3], Yuki Tanaka[3], Mikio Kandori[3], Toru Yoshie[3], and Yasuto Hijikata[,1]**

[1] Saitama University, Sakuraku, Saitama 338-8570, Japan
[2] National Institutes for Quantum and Radiological Science and Technology (QST), Takasaki 370-1292, Japan
[3] Sanken Electric Co., Ltd., Niiza, Saitama 352-8666, Japan

Received 17 June 2016, revised 11 January 2017, accepted 16 January 2017
Published online 00 Month 2017

Keywords device design, gamma radiation, MOSFET, radiation resistance, SiC

* Corresponding author: e-mail: mitomo@opt.ees.saitama-u.ac.jp, Phone: +81 488 583 465, Fax: +81 488 580 940
** e-mail yasuto@opt.ees.saitama-u.ac.jp, Phone: +81 488 583 822, Fax: +81 488 583 822

In order to develop highly radiation-tolerant SiC MOSFETs, we investigated the dependence of the gamma-ray radiation response on the gate oxide thickness and nitridation processes, used for oxide growth and p-well implantation. SiC MOSFETs with a thick gate oxide (60 nm) showed a rapid decrease in the threshold voltage shift ΔV_{th} of more than 400 kGy, and transitioned to the normally-on state at lower doses than those with a thin gate oxide (35 nm). The MOSFETs with gate oxides treated with lower concentrations of N_2O (10%) demonstrated a higher radiation tolerance (ΔV_{th}, channel mobility, and subthreshold swing) than with a 100% N_2O treatment. The MOSFETs with more p-well implantation steps (three steps) showed a smaller negative shift of the threshold voltage relative to those implanted with two steps.

1 Introduction Silicon carbide (SiC) is one of the most promising semiconductor materials for the fabrication of radiation-hardened (rad-hard) devices because of its high radiation resistance [1–8]. Among such rad-hard devices, the SiC metal-oxide-semiconductor field effect transistor (MOSFET) has attracted considerable attention as a power device for use in highly radiative conditions such as the decommissioning of nuclear power plants, because it is easy to obtain a normally-off characteristic and a very low power loss. Thus, there have been several reports describing the effects of gamma-ray irradiation on SiC MOSFETs [9–16]. According to these reports, the main cause of degradation in SiC MOSFETs under gamma-ray irradiation is a shift of the drain current (I_d)−gate voltage (V_g) characteristic toward the negative voltage side, due to positive charges generated in the gate oxide. The process of positive charge generation due to gamma-ray irradiation is believed to occur as follows [17]: when a MOSFET is irradiated with gamma-rays, electron-hole pairs are created in the gate oxide (SiO_2). Although some of these electron-hole pairs recombine, holes are far less mobile than electrons and most of them are trapped at defects near the oxide/semiconductor interface, resulting in positive oxide-fixed charges. Moreover, it has been reported for Si MOSFET that while holes induced by gamma-rays travel through the oxide, some of them combine with hydrogen in the oxide to generate hydrogen ions (protons) [17]. Because these protons drift into the Si/SiO_2 and react with the hydrogen atoms terminated to the defects at the Si/SiO_2 interface, the termination is released, reactivating the interface defects. As a result, the I_d–V_g curve shifts toward the positive voltage side, which is the opposite direction from that of the oxide-fixed charge case.

Based on the degradation mechanism described above, it was found that the radiation response of a MOSFET depends predominantly on the dimensions of the gate oxide and the device fabrication process. In the case of Si MOSFETs, it has been reported that thinner gate oxides are more radiation tolerant. For SiC MOSFETs, their typical fabrication process should affect the radiation response. In recent years, nitridation of the gate oxide has been widely used to improve the channel mobility [18]. Nitridation might improve the gamma-ray radiation resistance of SiC MOSFETs because the Si–N bond is stronger than the Si–H bond [19, 20]. Furthermore, ion implantation of

acceptor impurity atoms is usually used to fabricate a p-well channel region in SiC MOSFETs. The quality of this channel region, that is, oxide/semiconductor interface, may affect the radiation tolerance.

In this report, we investigate the effects of the oxide thickness, gate oxide nitridation process, and p-well implantation conditions on the radiation resistance, in order to obtain the optimum structure for gamma-ray radiation resistant SiC-MOSFETs.

2 Experimental The samples used in this study were TO3P packaged 4H-SiC vertical MOSFETs. The blocking voltage for the MOSFETs was 1200 V and the rated current was 20 A. The doping concentration of the p-wells was approximately $1–2 \times 10^{18}\,\mathrm{cm}^{-3}$. We prepared five samples to compare the irradiation effect in terms of oxide thickness, nitrogen (N_2O) concentration (Post-oxidation-anneal (POA) was applied after the gate-oxide growth. The atmospheric concentration of N_2O in POA was 100 or 10%. In the case of the N_2O 10% condition, N_2O was diluted with Ar), and p-well implantation conditions. (The number of p-well implantation steps was changed. The 3-implantation-step process was the same as the 2-step process, but with a shallow implantation step added.) Figure 1 shows a schematic illustration of acceptor concentration versus distance from the SiC substrate surface. As shown in the figure, the acceptor concentration at the substrate surface differed between two steps and three steps of p-well implantation (hereafter, denoted as "2-step p-well" and "3-step p-well," respectively.) The specifications of these samples are listed in Table 1. In the table, the number "2-step" and "3-step" denote the 2-step ion-implantation process and the 3-step ion-implantation process, respectively.

The MOSFETs were irradiated with gamma-rays from a ^{60}Co source, at dose rates between 1 and 10 kGy(SiO_2)/h, in an N_2 atmosphere, at room temperature (RT). During the irradiation, no bias was applied to the MOSFET electrodes. Before and after irradiation, the drain current (I_d)–gate voltage (V_g) characteristics were measured in air at RT in the dark. The samples were not irradiated continuously.

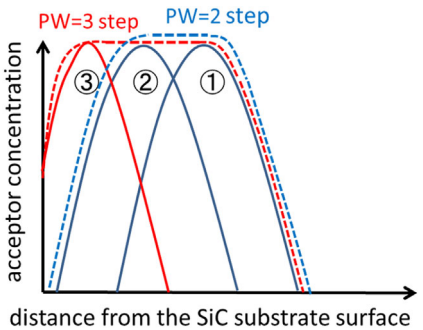

Figure 1 Schematic of acceptor concentration verses distance from the SiC substrate surface. The blue line indicates a 2-step p-well, and the red line indicates a 3-step p-well.

Table 1 Experimental samples.

gate oxide thickness (nm)	35		60	45	
N_2O concentration (%)	100				10
p-well implantation	2-step	3-step	2-step	3-step	2-step
sample notation	A	B	C	D	E

There were a few tens of hours between each irradiation, and the measurements were carried out during this interval. We observed the samples after an interval of 1 month, and no significant changes were found.

The value of V_{th} was estimated from the intersection between the V_g-axis and a line extrapolated from the curve of the square root of I_d vs. V_g in the saturation region (where W is the gate width and L is the gate length.):

$$I_d = \mu \frac{W}{2L} C_{ox} (V_g - V_{th})^2 \ , \tag{1}$$

$$\sqrt{I_d} = \sqrt{\mu \frac{W}{2L} C_{ox}} V_g - \sqrt{\mu \frac{W}{2L} C_{ox}} V_{th} \ , \tag{2}$$

The channel mobility was estimated from the slope of the I_d-V_g characteristics, where the resistance of the n-type epitaxial layer was assumed to be negligible. That is,

$$\frac{\partial I_d}{\partial V_g} = \frac{W}{L} \mu_n C_{ox} V_d \ , \tag{3}$$

$$\mu_n = \frac{L}{W} \frac{1}{C_{ox} V_d} \frac{\partial I_d}{\partial V_g} \ , \tag{4}$$

where W is the gate width and L is the gate length.

The swing (S-factor) was estimated from the increment of V_g over the range of $I_d = 10^{-3}$–10^{-4} A:

$$\text{swing} = \frac{\Delta V_g}{\log_{10} 10^{-3} - \log_{10} 10^{-4}} = \Delta V_g [\mathrm{V}/dec] \ , \tag{5}$$

The voltage shifts due to positive oxide-fixed charge and interface-trapped charge (ΔV_{not} and ΔV_{nit}, respectively) were estimated by extrapolating the I_d–V_g curve to the midgap current I_{mg}, using the subthreshold slope [21, 22]. For the separation of ΔV_{th} into ΔV_{not} and ΔV_{nit}, it is necessary to extract ΔV_{not} first. ΔV_{not} can be obtained from ΔV_{mg}, i.e.,

$$\Delta V_{not} = \Delta V_{mg} \ , \tag{6}$$

where V_{mg} is the value of V_g when $I_d = I_{mg}$.

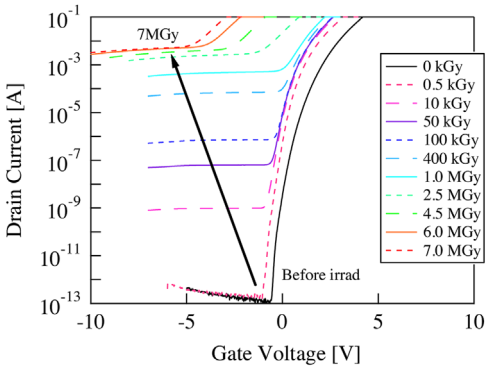

Figure 2 I_d–V_g curves in the subthreshold region for an SiCMOSFET (sample A), before and after gamma-ray irradiation up to 7 MGy.

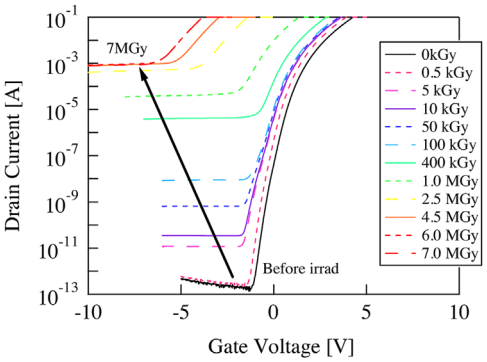

Figure 4 I_d–V_g curves in the subthreshold region for an SiCMOSFET (sample C), before and after gamma-ray irradiation up to 7 MGy.

Furthermore, the value of I_{mg} was estimated using

$$I_d = 2^{1/2}\mu(W/L)(qN_AL_B/\beta)(n_i/N_A)^2\exp(\beta\phi_s)(\beta\phi_s)^{-1/2}\ , \quad (7)$$

where N_A, n_i, ϕ_s, and L_B are the acceptor (or donor) concentration in the channel region, the intrinsic carrier concentration, the band bending at the surface, and the Debye length. According to Eq. (7), the value of I_{mg} for 4H-SiC is in the order of approximately 10^{-30} A. Provided that ΔV_{th} is the sum of ΔV_{not} and ΔV_{nit}, ΔV_{nit} can be obtained from the following equation [23]:

$$\Delta V_{nit} = \Delta V_{th} - \Delta V_{not}\ . \quad (8)$$

3 Results and discussion

3.1 Drain current–gate voltage characteristic

Figures 2–6 show I_d–V_g curves at various irradiation doses for samples A–E. In these figures, the curves shift to the negative voltage side with increasing irradiation dose, indicating the generation of positive charges in the gate oxides during irradiation. The figures also indicate that the leakage current (I_d in the negative V_g region) increased with increasing dose. Our recent investigations found that there was a structural leakage path in the electrical isolator that was sensitive to gamma-ray irradiation in the vicinity of the electrodes in these samples. Therefore, because the leakage current is not a fundamental problem but a problem of device layout, we will not discuss it further herein.

3.2 Gate oxide thickness

Figure 7 shows the dependence of the threshold voltage shift ΔV_{th} on irradiation dose for MOSFETs with different gate oxide thicknesses (samples A and C), where ΔV_{th} is the difference between the threshold voltage and the initial (non-irradiated) value. As shown in Fig. 7, ΔV_{th} for both MOSFETs has shifted to the negative voltage side after irradiation. This indicates that the oxide-trapped positive charges generated by the irradiation have accumulated in the oxide with increasing absorbed dose. Although the ΔV_{th} values for both MOSFETs were changed very little after doses of hundreds of kGy, they decreased significantly above 1 MGy. The ΔV_{th} values of thinner oxides began to decrease at higher doses than those of thicker oxides. Thus, SiC MOSFETs with thinner oxides

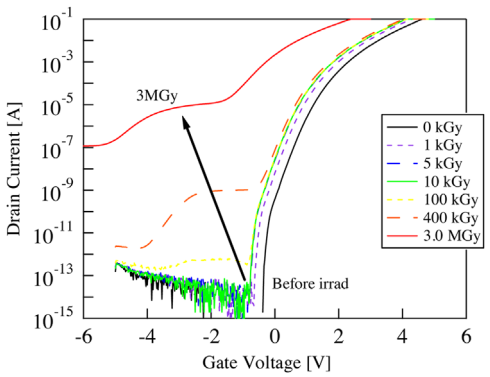

Figure 3 I_d–V_g curves in the subthreshold region for an SiCMOSFET (sample B), before and after gamma-ray irradiation up to 3 MGy.

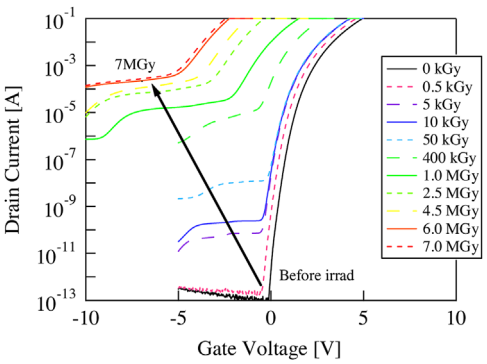

Figure 5 I_d–V_g curves in the subthreshold region for an SiCMOSFET (sample D), before and after gamma-ray irradiation up to 7 MGy.

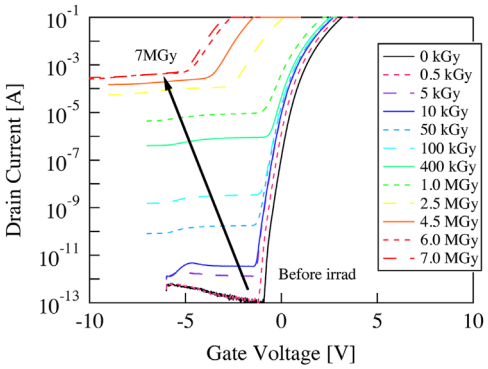

Figure 6 I_d–V_g curves in the subthreshold region for an SiCMOSFET (sample E), before and after gamma-ray irradiation up to 7 MGy.

had a higher radiation tolerance. It is probable that the number of positive charges generated in thinner oxides is smaller than that in thicker ones, and/or these positive charges easily escape from the hole traps in thinner oxides. It should be noted that both MOSFETs showed normally-off characteristics, even after 1 MGy of irradiation. Therefore, it is inferred that SiC MOSFETs generally have higher radiation tolerances than Si MOSFETs [17].

Figure 8 shows the dependence of the normalized channel mobility (normalized by the initial, non-irradiated value) on the irradiation dose for MOSFETs with 35 and 60 nm thick oxides. The channel mobility was calculated as dI_d/dV_g at $V_d = 1$ V. The normalized mobility at 60 nm hardly changed after irradiation up to 1 MGy, suggesting that interface traps between the gate oxide and SiC, that act as scattering centers for carriers in the channel, did not significantly increase in the low-dose region. However, after 1 MGy of irradiation, the normalized mobility increased, implying that the number of interface states decreased. In contrast, the channel mobility for 35 nm steadily increased. Therefore, for thinner oxides, the interface is more stable and more resistant to irradiation.

Figure 9 shows the dependence of swing on irradiation dose for MOSFETs with oxide thicknesses of 35 and 60 nm.

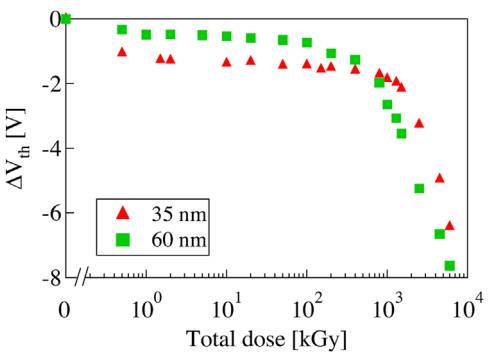

Figure 7 Threshold voltage of SiC MOSFETs as a function of gamma-ray dose. Triangles and squares indicate results obtained for 35- and 60-nm-thick oxides, respectively.

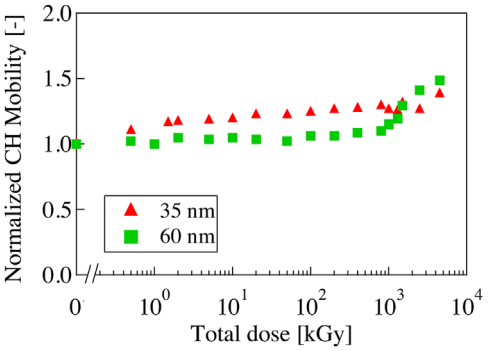

Figure 8 Normalized channel mobility of SiC MOSFETs as a function of gamma-ray dose. Triangles and squares indicate results obtained for 35- and 60-nm-thick oxides, respectively. The channel mobility was calculated as dI_d/dV_g ($V_d = 1$ V). The channel mobility values shown were normalized by the initial (non-irradiated) value.

For 35 nm, the swing immediately decreased at 0.5 kGy, but the swing for both MOSFETs remained relatively unchanged until approximately 400 kGy. Therefore, the interfaces of both MOSFETs were relatively stable below 400 kGy, but deteriorated at higher doses.

It has been reported for Si MOSFET with SiO_2 gate oxides that, as in SiC MOSFETs, a higher radiation tolerance is obtained with a thinner oxide because the thinner oxide suppresses carrier trapping [17]. Figure 10 shows the dose dependence of the voltage shift due to the charges trapped in the oxide and in the interface state, for different gate oxide thicknesses. As shown in the figure, our results also revealed that thinner oxides in SiC MOSFETs suppress the generation of positive charges in the oxide and improve the radiation tolerance.

Figure 11 shows the total dose dependence of the voltage shift due to charges trapped in the oxide and in the interface state for gate oxide thicknesses of 35 and 60 nm. In general, the threshold voltage of a SiC MOSFET changes like a linear function [24]. Accordingly, we calculated the slope of a linear fit of the threshold voltage. This slope was −0.82 V/MGy for

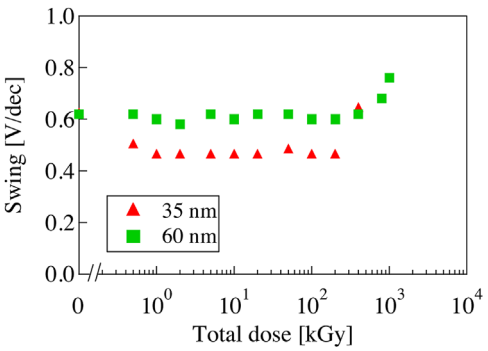

Figure 9 Swing of SiC MOSFETs as a function of gamma-ray dose. Triangles and squares indicate results obtained for 35 and 60 nm thick oxides, respectively. The swing was calculated for the range $I_d = 10^{-3}$–10^{-4} A.

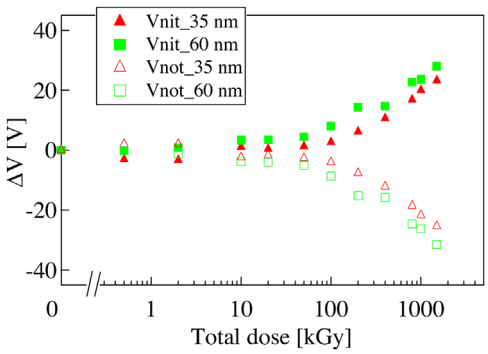

Figure 10 Total dose dependence of the voltage shift due to charges trapped in the oxide and interface state. Triangles and squares denote gate thicknesses of 35 and 60 nm, respectively. Filled and unfilled symbols indicate values for charges trapped in the interface state and in the oxide, respectively.

35 nm and −1.50 V/MGy for 60 nm. The ratio (1.82) is close to the ratio of oxide thicknesses 60/35 (1.74), indicating that the difference in oxide thickness directly corresponds to the degradation rate of the threshold voltage.

3.3 Nitrogen concentration Figure 12 shows the threshold voltage shift ΔV_{th} on irradiation dose for different nitridation conditions (sample D and E). As shown in Fig. 12, ΔV_{th} for both MOSFETs shifted to the negative voltage side after irradiation. Although ΔV_{th} for both MOSFETs did change slightly up to 100 kGy, ΔV_{th} for a 100% N_2O concentration decreased significantly above 100 kGy. Thus, the lower nitrogen concentration sample had a higher radiation tolerance. We suppose that excess nitrogen near/at the interface weakened the bonding network.

Figure 13 shows the dependence of normalized channel mobility on irradiation dose for N_2O concentrations of 100 and 10%. Up to 400 kGy, both mobilities were unchanged, but after 400 kGy irradiation, the mobility in the 10% samples began to increase. Moreover, when the dose reached approximately 1 MGy, the mobility for 100% also increased.

Figure 14 shows the dependence of swing on irradiation dose for N_2O concentrations of 100 and 10%. Although the

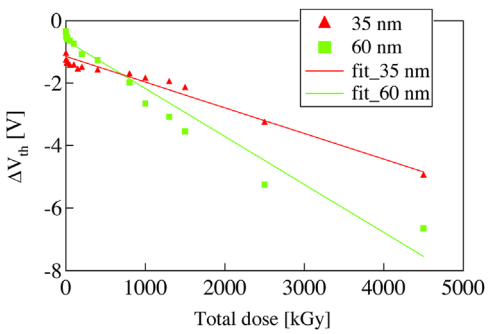

Figure 11 Threshold voltage of SiC MOSFETs as a function of gamma-ray dose. Triangles and squares indicate results obtained from oxide thicknesses of 35 nm and 60 nm, respectively. The red line is a fit of the threshold voltage shift of 35 nm, and the green line is a fit for 60 nm.

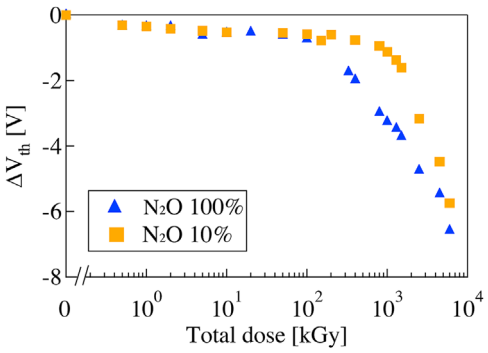

Figure 12 Threshold voltage shift of SiC MOSFETs as a function of gamma-ray dose. Triangles and squares indicate N_2O concentrations of 100 and 10%, respectively.

swing for both MOSFETs changed very little up to 400 kGy, the 10% N_2O MOSFET had a lower (better) value for all doses than the 100% N_2O MOSFET. To reduce the interface state, the lower nitrogen concentration should be selected. In general, the behavior of the swing is consistent with that of the channel mobility. However, the channel mobility is also affected by the threshold voltage. Therefore, the fact that the dose dependence of the swing was slightly different from that of the channel mobility may be due to the difference in dose dependence of V_{th}.

It has been considered that nitridation treatment could remove residual carbon from the SiO_2/SiC interface and reduce the interface trap density [18]. Moreover, a nitrogen atom with a lone pair of electrons acts as a negative charge, leading to a high threshold voltage. However, the initial value of threshold voltage for the higher N_2O concentration (100%) sample was larger (2.85 V) than that for the lower concentration (10%) sample (1.90 V). This demonstrates that the sample treated with a higher concentration of N_2O had a larger margin leading up to the normally-on state. However, after irradiation of 1 MGy, the sample treated with a higher concentration generated more positive charges in the gate oxide and deteriorated more quickly. We believe

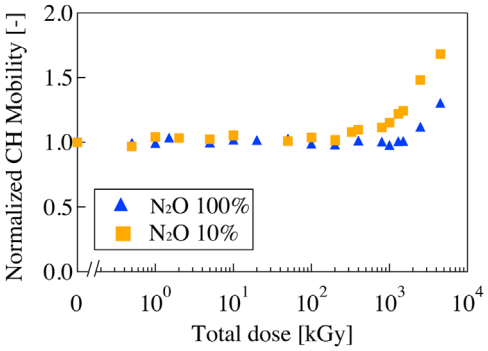

Figure 13 Normalized channel mobility of SiC MOSFETs as a function of gamma-ray dose. Triangles and squares indicate N_2O concentrations of 100 and 10%, respectively. Channel mobility was calculated as dV_g/dI_d ($V_d = 1$ V). The channel mobility values shown were normalized by their initial values.

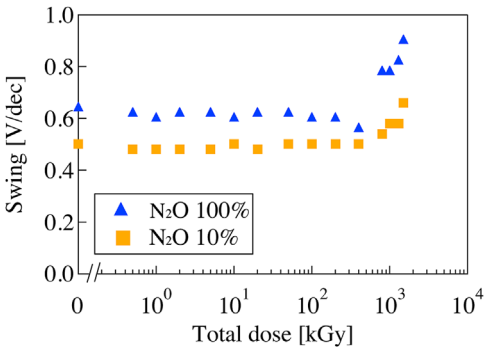

Figure 14 Swing of SiC MOSFETs as a function of gamma-ray dose. Triangles and squares indicate N_2O concentrations of 100 and 10%, respectively. The swing was calculated in the range of $I_d = 10^{-3}$–10^{-4} A.

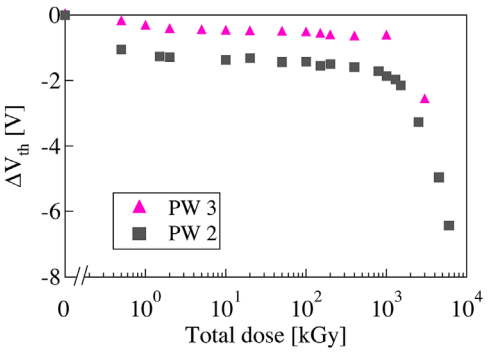

Figure 16 Threshold voltage shift of SiC MOSFETs as a function of gamma-ray dose. Triangles and squares indicate 3-step and 2-step p-wells, respectively.

that this is because nitrogen in the oxide generates hole-trapping defects that capture holes generated by gamma-rays. Figure 15 shows the total dose dependence of the voltage shift due to charges trapped in the oxide and in the interface state for N_2O concentrations of 100 and 10%. It is clear that the trap densities for both the oxide and the interface were lower in the case of low N_2O concentration. Therefore, from the point of view of radiation tolerance, there is an advantage for samples treated with lower N_2O concentrations (Fig. 15).

3.4 P-well implantation Figure 16 shows the dependence of ΔV_{th} on irradiation dose for 2-step and 3-step p-well MOSFETs (Samples A and B, respectively). Although ΔV_{th} for the 2-step p-well decreased by 1 V at 0.5 kGy, both ΔV_{th} curves had a similar dependence on total dose. Therefore, it is presumed that in terms of threshold voltage, the 3-step p-well MOSFET had a higher gamma-ray resistance than the 2-step.

Figure 17 shows the dependence of normalized channel mobility on irradiation dose for 2- and 3-step p-well SiC MOSFETs. The normalized channel mobility for the 2-step p-well increased with increasing dose. It is probable that, because the 2-step p-well MOSFET had a higher donor concentration at the surface, a higher electron density was obtained in the channel region. It is also possible that using fewer implantation steps might reduce the defects generated by impurities and/or irradiation.

Figure 18 shows the dependence of swing on irradiation dose for 2-step and 3-step p-well SiC MOSFETs. As the swing of the 3-step p-well MOSFET did not change at all after irradiation, the interface state density could have been unchanged. In contrast, the swing for the 2-step p-well MOSFET initially decreased but then increased at 400 kGy. The decreased swing in the low-dose region is responsible for annealing the interface state. The MOSFETs with fewer p-well implantation steps had somewhat better interface characteristics after gamma-ray irradiation.

The results obtained from this study can be explained by considering that a higher surface concentration of acceptor impurities forms more defects at the surface. This causes deterioration of the interface characteristics. On the other hand, as shown in Fig. 1, a higher surface concentration suppresses the negative shift of the threshold voltage. Although there is a trade-off between the threshold voltage

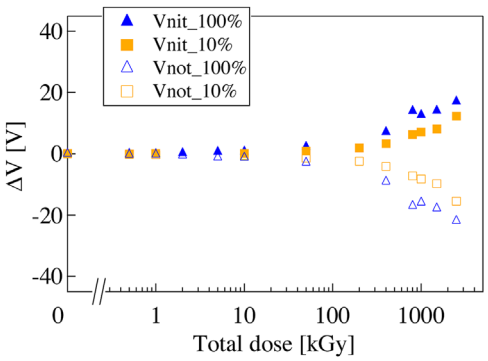

Figure 15 Total dose dependence of voltage shift due to charges trapped in the oxide and interface state. Triangles and squares indicate N_2O concentrations of 100 and 10%, respectively. Filled and unfilled symbols indicate values for charges trapped in the interface state and in the oxide, respectively.

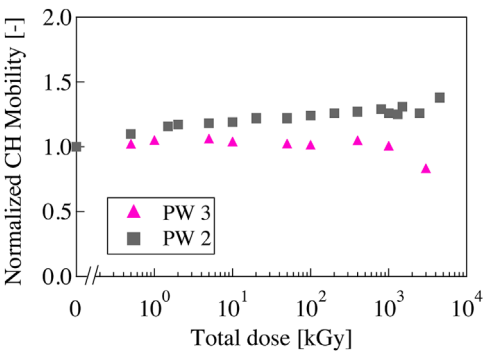

Figure 17 Normalized channel mobility of SiC MOSFETs as a function of gamma-ray dose. Triangles and squares indicate 3-step and 2-step p-well implantations, respectively. The channel mobility was calculated as dI_d/dV_g ($V_d = 1$ V). The channel mobility values shown were normalized by their initial value.

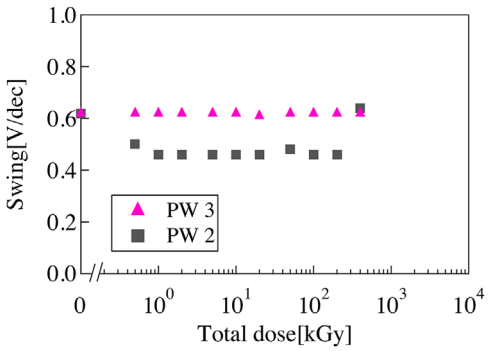

Figure 18 The swing of SiC MOSFETs as a function of gamma-ray dose. Triangles and squares indicate 3-step and 2-step p-well implantations, respectively. The swing was calculated in the range of $I_d = 10^{-3}$–10^{-4} A.

shift and interface characteristics, the sample with more implantation steps, that is, a higher acceptor concentration at the substrate surface, had a wider margin leading up to the normally-on state and a higher radiation tolerance.

4 Conclusions To develop highly radiation tolerant power devices, gamma-ray radiation responses of vertical 4H-SiC MOSFETs with various device structures were investigated. We compared MOSFETs with different gate oxide thicknesses, nitridation processes, and numbers of p-well implantation steps to obtain an optimum device structure in terms of radiation tolerance. We found that radiation tolerant SiC MOSFETs can be obtained with thinner gate oxides, lower nitrogen concentrations in the nitridation process, and higher acceptor concentrations at the p-well surface.

Acknowledgements This study was partially supported by the Nuclear Science Research Initiative of Japan.

References

[1] C. Brisset, O. Noblanc, C. Picard, F. Joffre, and C. Brylinski, IEEE Trans. Nucl. Sci. **47**, 598–603 (2000).
[2] T. Nishijima, T. Ohshima, and K. K. Lee, Nucl. Instr. Meth. Phys. Res. B **190**, 329–334 (2002).
[3] F. Nava, E. Vittone, P. Vanni, G. Verzellesi, P. G. Fuochi, C. Lazien, and M. Glaser, Nucl. Instr. Meth. Phys. Res. A **505**, 645–655 (2003).
[4] T. Ohshima, K. K. Lee, S. Onoda, T. Kamiya, M. Oikawa, J. S. Laird, T. Hirao, and H. Itoh, Nucl. Instr. Meth. Phys. Res. B **206**, 979–983 (2003).
[5] P. J. Sellin, and J. Vaitkuset, Nucl. Instr. Meth Phys. Res. A **557**, 479–489 (2006).
[6] T. Ohshima, T. Sato, M. Oizawa, S. Onoda, and H. Tto, Mater. Sci. Forum **527**, 1347–1350 (2006).
[7] S. Onoda, N. Iwamoto, S. Ono, S. Katakami, M. Arai, K. Kawano, and T. Ohshima, IEEE Trans. Nucl. Sci. **56**, 3218–3222 (2009).
[8] Y. Tanaka, S. Onoda, A. Takatsuka, T. Ohshima, and T. Yatsuo, Mater. Sci. Forum **645-648**, 941–944 (2010).
[9] T. Ohshima, M. Yoshikawa, H. Itoh, Y. Aoki, and I. Nashiyama, J. Appl. Phys. **37**, L1002–L1004 (1998).
[10] T. Ohshima, H. Itoh, and M. Yoshikawa, J. Appl. Phys. **90**(6), 3038–3041 (2001).
[11] K. K. Lee, T. Ohshima, and H. Itoh, Mater. Sci. Forum **389-393**, 1097–1100 (2002).
[12] K. K. Lee, T. Ohshima, and H. Itoh, IEEE Trans. Nucl. Sci. **50**, 194–200 (2003).
[13] S. Onoda, T. Makino, N. Iwamoto, G. Vizkelethy, K. Kojima, S. Nozaki, and T. Ohshima, IEEE Trans. Nucl. Sci. **57**, 3373–3379 (2010).
[14] T. Yokoseki, H. Abe, T. Makino, S. Onoda, Y. Tanaka, M. Kandori, T. Yoshie, Y. Hijikata, and T. Ohshima, Mater. Sci. Forum **821-823**, 705–708 (2015).
[15] T. Ohshima, T. Yokoseki, K. Murata, T. Matsuda, S. Mitomo, H. Abe, T. Makino, S. Onoda, Y. Hijikata, Y. Tanaka, M. Kandori, S. Okubo, and T. Yoshie, Jpn. J. Appl. Phys. **55**, 01AD01 (2015).
[16] A. Takeyama, T. Matsuda, T. Yokoseki, S. Mitomo, K. Murata, T. Makino, S. Onoda, S. Okubo, Y. Tanaka, and M. Kandori, Jpn. J. Appl. Phys. **55**, 104101 (2016).
[17] J. R. Schwank, IEEE Nuclear and Space Radiation Effects Conference, Section III (2002).
[18] J. Rozen, in: Physics and Technology of Silicon Carbide Devices, edited by Y. Hijikata, (InTech, Janeza Trdine 9, 51000 Rijeka, Croatia, 2013), Section 3, chap. 10.
[19] T. Chen, Z. Luo, J. D. Cressler, T. F. Isaac-Smith, J. R. Williams, G. Chung, and S. D. Clark, Solid-State Electron. **46**, 2231–2235 (2002).
[20] C. Sah, Fundamentals of Solid-state Electronics Solution Manual (World Scientific Publishing Company, 1996), p.121.
[21] P. J. McWhorter and P. S. Winokur, Appl. Phys. Lett. **48**, 133–135 (1986).
[22] E. W. Enlow, R. L. Pease, and D. R. Alexander, Defense Nuclear Agency **861**, AD–A221 (1990).
[23] T. Ohshima, S. Onoda, N. Iwamoto, T. Makino, M. Arai, and Y. Tanaka, in: Physics and Technology of Silicon Carbide Devices, edited by Y. Hijikata, (InTech, Janeza Trdine 9, 51000 Rijeka, Croatia, 2013), chap.16.
[24] A. Akturk, J. M. McGarrity, S. Potbhare, and N. Goldsman, IEEE Trans. Nucl Sci. **59**, 3258–3264 (2012).

